Supporting Information

Rapid, *In-situ* Synthesis of High Capacity Battery Anodes Through High Temperature Radiation-based Thermal Shock

Yanan Chen[1, (a)], Yiju Li[1, (a)], Yanbin Wang[1], Valencia A. Danner[1], Jiaqi Dai[1], Steven D. Lacey[1], Yonggang Yao[1], Liangbing Hu[1,*]

[1]Department of Materials Science and Engineering, University of Maryland, College Park,

Maryland, 20742

* Corresponding author Email: binghu@umd.edu

Experimental Section

Preparation of reduced graphene oxide-Si microparticles (RGO-SiMPs) film: The graphene oxide (GO) solution was synthesized by the improved Hummer's method.[1] Specifically, 1.5 g of natural graphite flakes were added into a 200 mL mixed acid solution of H_2SO_4/H_3PO_4 (volume ratio 9:1). 9 g of $KMnO_4$ was slowly added to the solution before heating and stirring at 50^oC for 12 h. The solution was cooled to room temperature and poured into 200 mL of ice mixed with 3 mL of H_2O_2. The mixture was washed several times with a 5% HCl solution and distilled water by centrifugation. The GO solution was diluted with distilled water to obtain a 2.5 mg mL^{-1} concentration. The SiMPs solution was prepared by adding 30 mg of microsized Si powders into 12 mL ethanol, followed by sonication for 1 minute. The GO-SiMPs solution was obtained by mixing the as-prepared GO solution and Si micropowder solution with a weight ratio of 1:1. The 1:1 solution was mixed using a Tube Vertex Mixer for 1 minute and sonicated for ~10 seconds. A uniform GO-SiMPs suspension with GO sheets and dispersed Si microparticles can be obtained due to the electrostatic interactions between the GO sheets and the Si micropowder.

A freestanding GO-SiMPs film (35 mm in diameter) was obtained by filtering the as-prepared GO-SiMPs solution through a 0.65 μm pore-sized membrane (Millipore, U.S.A) under vacuum. The GO-SiMPs film can be detached from the membrane naturally after drying in air for 10 h. The GO-SiMPs film was then thermally reduced in a tube furnace under a H_2/Ar (5%/95%) atmosphere with a 300^oC hold for 1 h and a ramp rate of $3^oC/min$.

Characterization methods: The morphologies of the samples were examined by a Hitachi SU-70 field emission scanning electron microscope (SEM), and a JEOL JEM 2100 transmission electron microscope (TEM) at an accelerating voltage of 200 kV. Crystal structure analysis was

performed via X-ray diffraction (XRD) on a D8 Advanced (Bruker AXS, WI, USA). Micro-Raman analysis was performed with a Horiba Yvon LabRam ARAMIS confocal Raman microscope with a 633 nm He-Ne laser. Thermogravimetric analysis (TGA) was performed using a simultaneous differential scanning calorimeter (DSC)/TGA instrument (SDT Q600, TA instruments). The samples were heated in air (100 mL/min flow rate) from room temperature to 800°C at 10°C/min. An integrating sphere connected to a UV-Vis-NIR spectrometer with a wider working range (Lambda 1050) was employed to measure the reflectance and transmittance of the RGO-SiMPs film. Absorption was determined using the following equation: 1 – transmission – reflection.

Temperature characterization: The spectral measurement system was calibrated by a NIST-traceable light source to ensure accuracy. A spectrometer-coupled optical fiber with a 400 μm diameter was aligned on top of a freestanding RGO paper (heater). The emission spectrum of the testing heater was then measured and recorded (Figure S1). The recorded emission spectrum of the heater was then fitted to the Blackbody radiation equation, as shown below, to extract the in-situ temperature of the heat source:

$$I_\lambda(\lambda,T) = \gamma \varepsilon_{gray} \frac{2hc^2}{\lambda^5 \left[\exp\left(\dfrac{hc}{\lambda k_B T} \right) - 1 \right]}$$

where ε_{gray}, k_B, h, c, and γ is the realistic range of emissivity, Boltzmann constant, Planck constant, speed of light and the scaling constant, respectively. Note that the unknown coupling factor between the RGO paper illumination and the input of the optical fiber was taken into

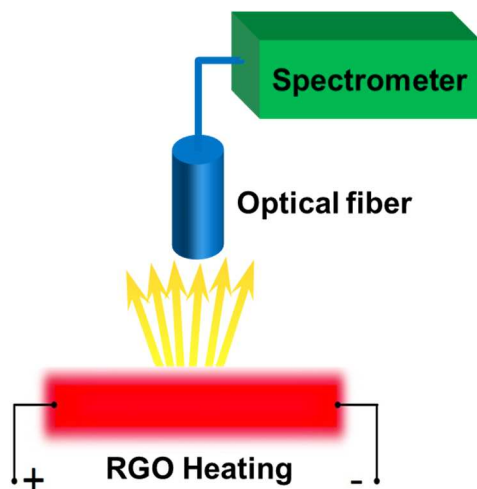account. By mathematically fitting each curve from Fig. 2d to Eq. (1), the temperature can be extracted.[2,3]

Figure S1. Schematic illustration of the setup used for quantifying the temperature of the RGO heater.

Battery performance evaluation: The electrochemical performance was investigated using CR 2032 coin cells. The as-prepared films were directly used as the working electrodes without the addition of binder or conductive agents. Lithium was used as the counter and reference electrode. The liquid electrolyte was 1 M LiPF$_6$ in ethylene carbonate/diethyl carbonate (EC: DEC = 1:1 by volume). All the cells were assembled in a high-purity argon-filled glovebox and tested using an Arbin battery test system. The galvanostatic charge-discharge tests were conducted in a voltage range of 0.01 V to 2.0 V versus Li/Li$^+$.

3D printing manufacturing: 3D printing was conducted by a benchtop robot (Fisnar F4200n) using a preprogrammed patterning procedure. The GO and GO-SiMPs inks were stored in separate syringes for the printing process. The GO-based ribbons were formed by printing the

GO-based inks via a 0.254 mm cylindrical nozzle with a horizontal speed of 50 mm/s. The ink flow was controlled by an air-powered fluid dispenser (DSP501N, Fisnar) and the printing pressure was adjusted to 60 psi to maintain a constant ink flow.

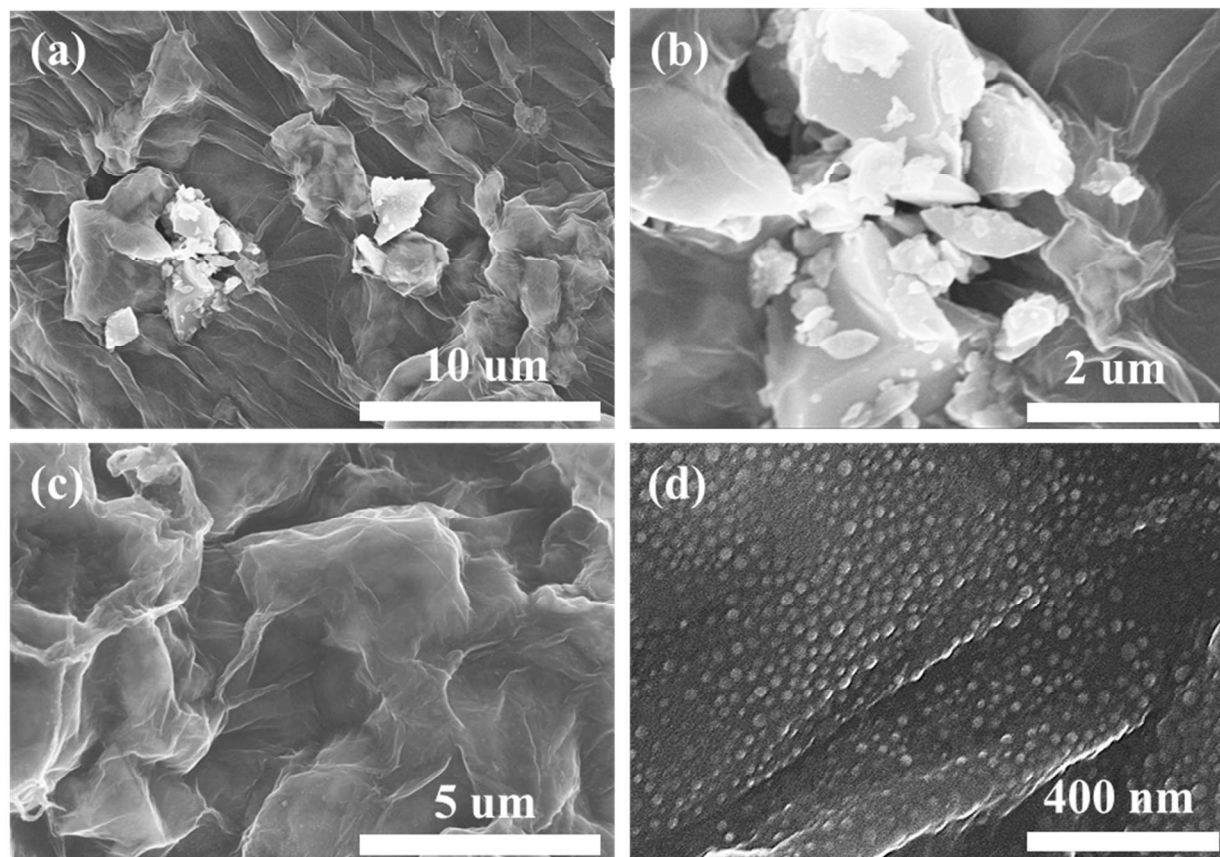**Characterization of RGO-Si before and after a high temperature thermal shock treatment**

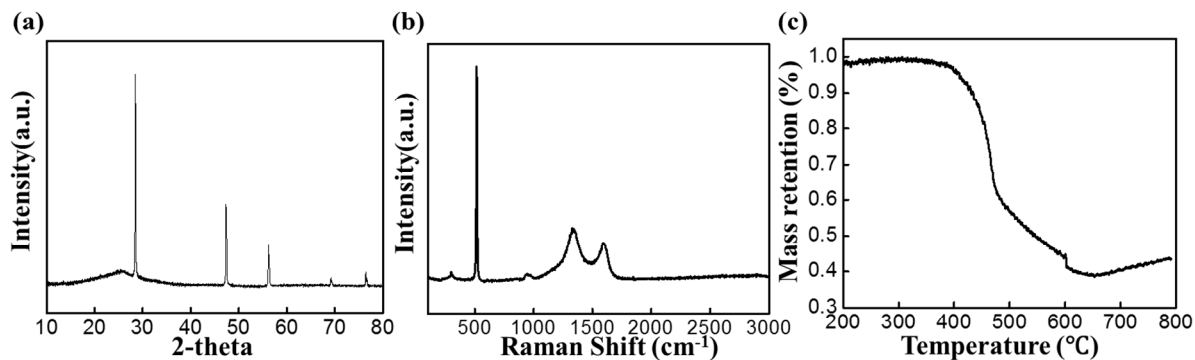**Figure S2.** SEM images of (a, b) RGO-SiMPs and (c, d) RGO-SiNPs after thermal shock at ~1800 K for 30s.

Figure S3. (a) Representative XRD patterns of RGO-SiNPs. Five sharp peaks appeared at 28°, 47°, 56°, 69°, and 76° which are assigned to the (111), (220), (311), (400), and (331) reflections

of crystalline silicon. A broad peak at 26° should be due to the presence of RGO. (b) Raman spectroscopy of RGO-SiNPs composite. (c) TGA curve of RGO-SiNPs. Silicon content is 39% in the RGO-SiNPs composite.
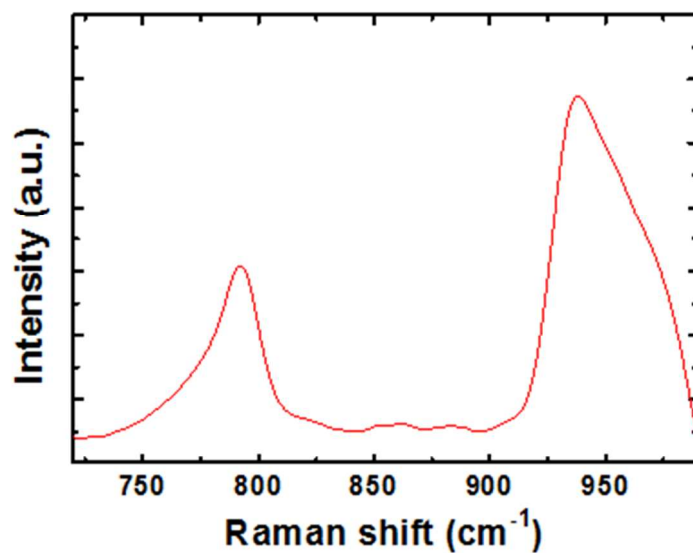

Figure S4. Raman spectroscopy of the RGO-SiNPs composite after thermal shock treatment at ~1900K for 30s. The peaks at 790 cm^{-1} and 940 cm^{-1} indicates the formation of silicon carbide.

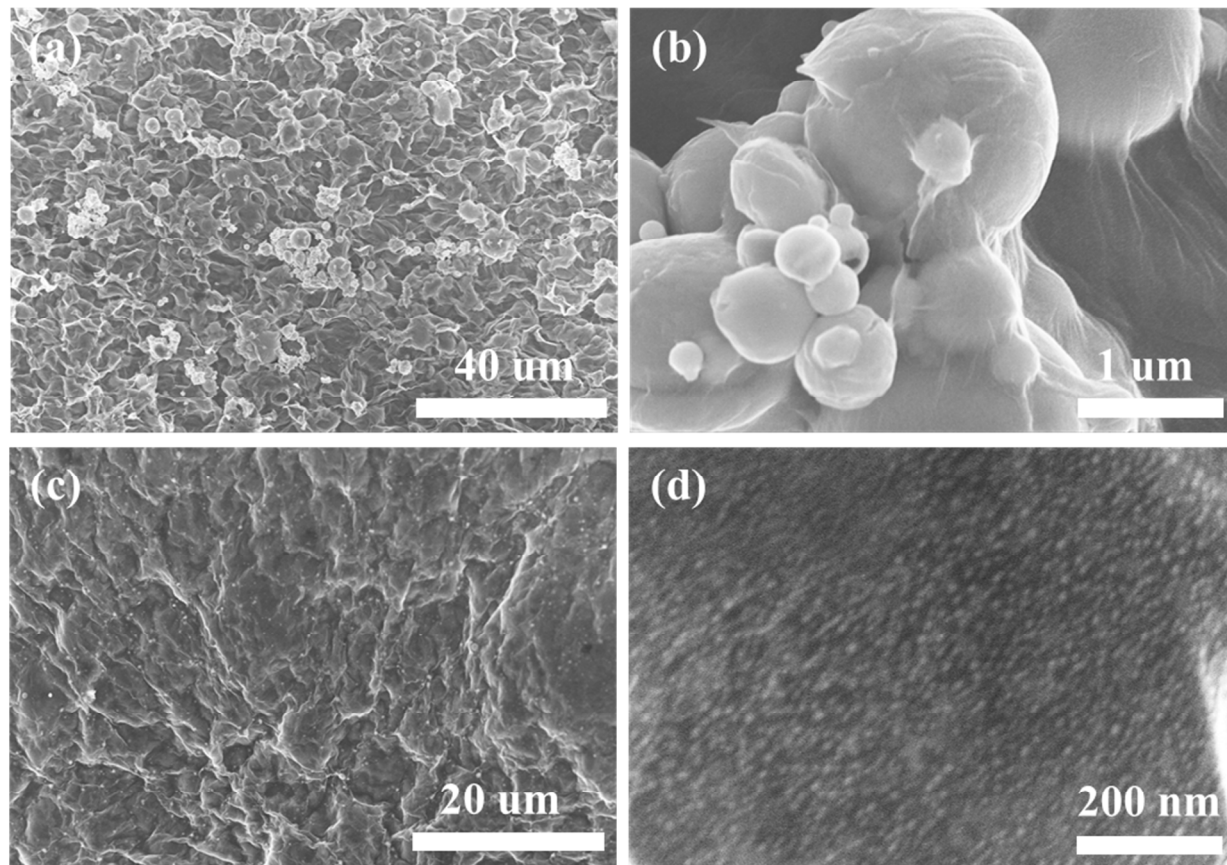**Characterization of RGO-Sn before and after a high temperature thermal shock treatment**

Figure S5. SEM images of (a, b) RGO-SnMPs and (c, d) RGO-SnNPs after thermal shock at ~1550 K for 30s.
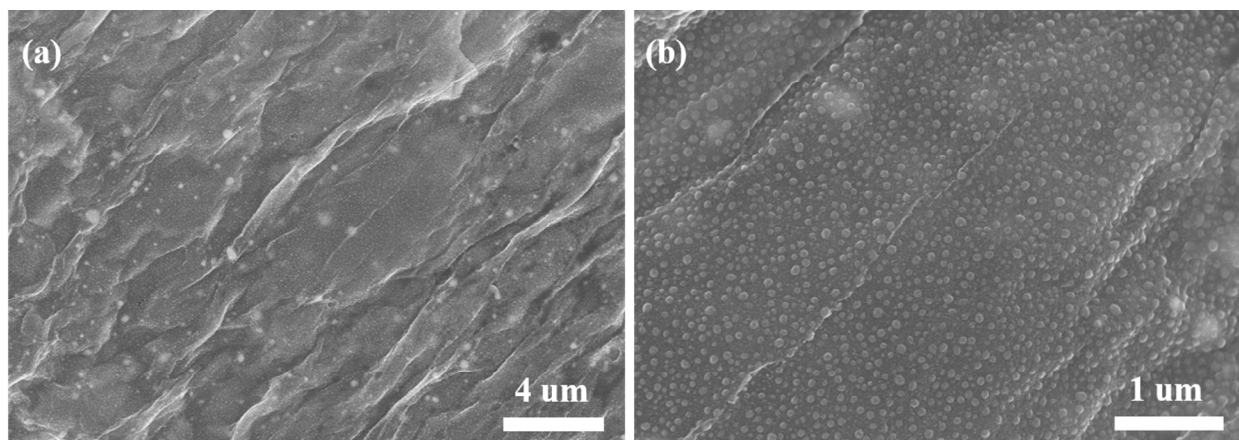
Figure S6. SEM images of (a) RGO-SnNPs after thermal shock at ~1550 K for 1h. (b) is a zoom-in image of (a).
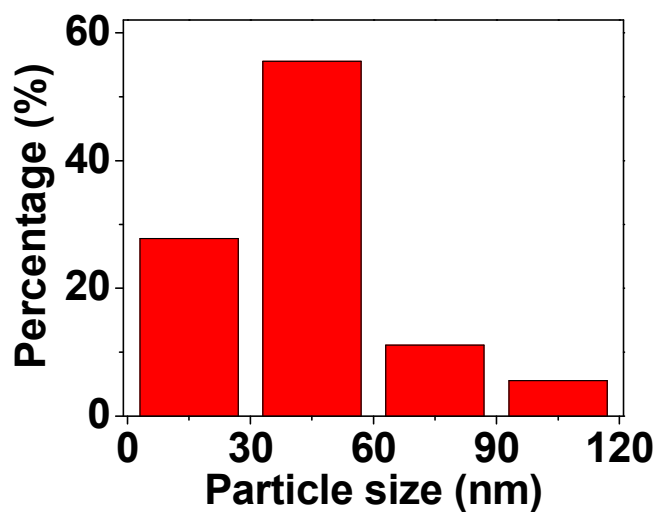

Figure S7. The statistical particle size distribution of SnNPs after thermal shock at ~1550 K for 1h.

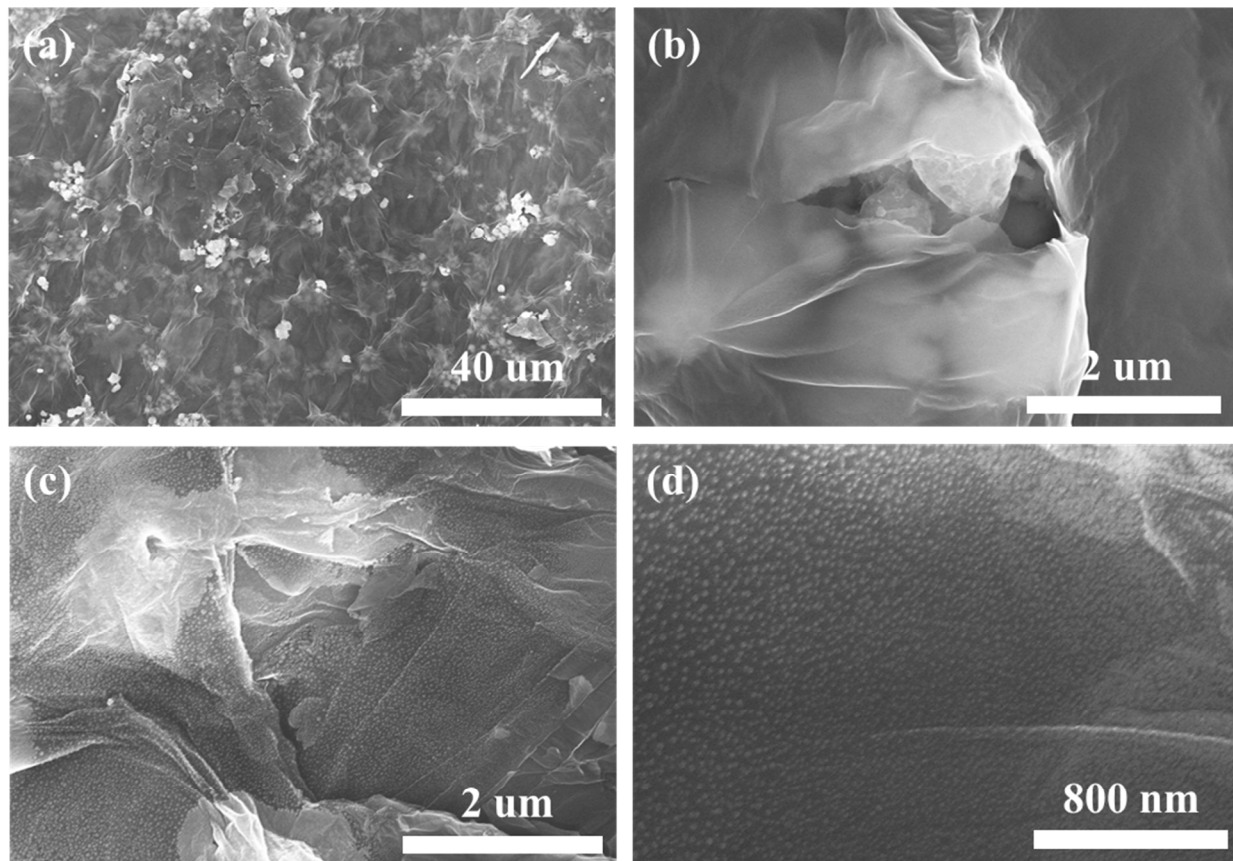**Characterization of RGO-Al before and after a high temperature thermal shock treatment**

Figure S8. SEM images of (a, b) RGO-AlMPs and (c, d) RGO-AlNPs after thermal shock treatment at ~1700 K for 30s.
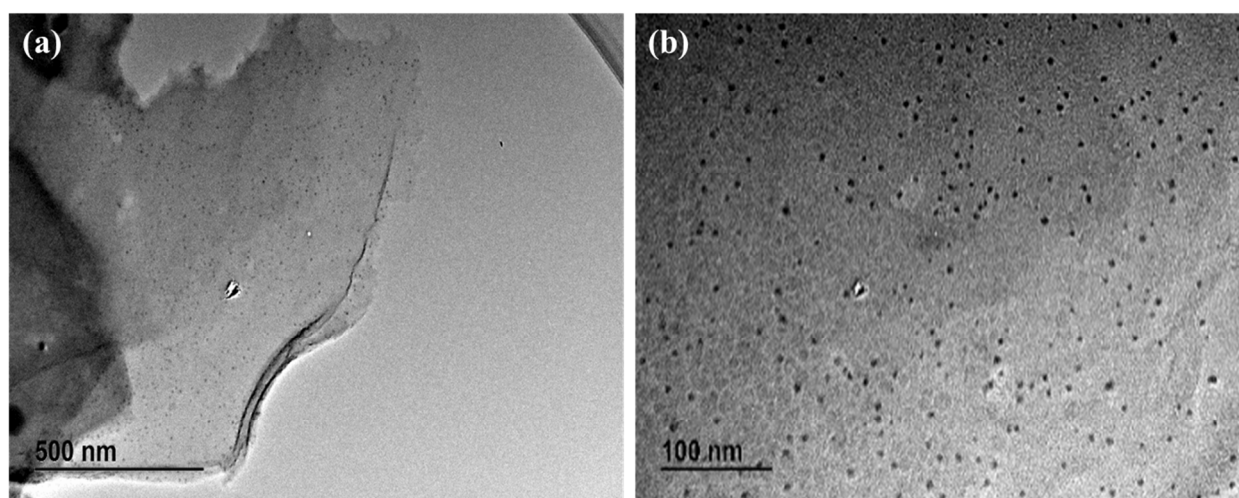

Figure S9. TEM images of (a, b) RGO-AlNPs after thermal shock treatment at ~1700 K for 30s.

Electrochemical performance of RGO-Sn before and after a high temperature thermal shock treatment
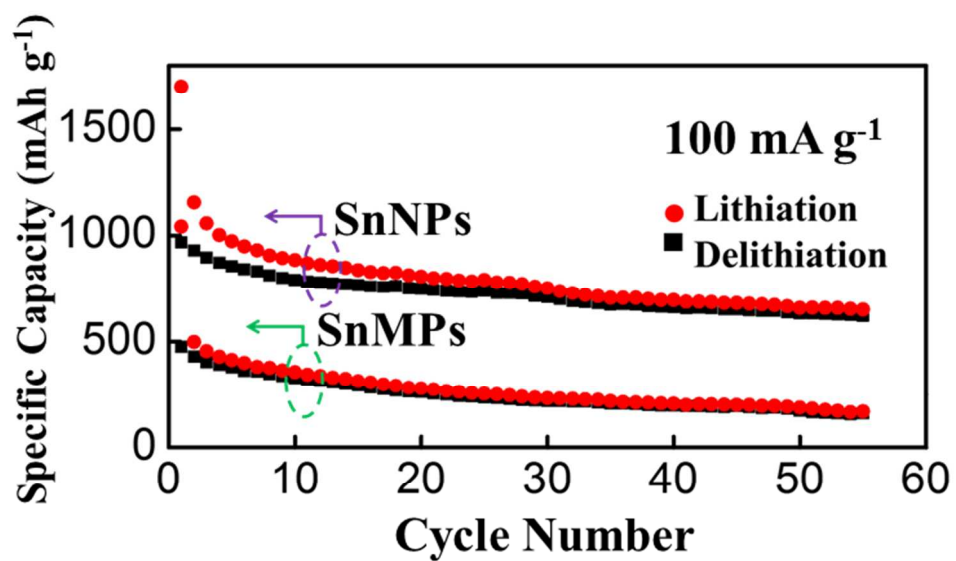

Figure S10. Cycling performance of RGO-SnNPs and RGO-SnMPs tested at 100 mA g^{-1}.

Rheological properties of GO-Si slurry

The rheological properties of the pure GO suspension with a concentration of 85 mg/mL, and the GO-Si composite with 10%wt Si addition are shown in Figure S11a, which display the apparent viscosity as a function of shear rate. The GO and GO-Si inks have an apparent viscosity ranging from 10^2 to 10^3 Pa·s at a shear rate of 1 s^{-1}. GO and GO-Si inks exhibit similar shear-thinning behavior, revealing that they are non-Newtonian fluids. The slurry is promising for 3D printing. Figure S11b depicts the storage and loss moduli of GO and GO-Si inks as a function of shear stress, which reflects the elastic and viscous properties of the printed inks. There are similar plateau and crossover regions for both inks in Figure S11b. In the plateau region, the storage modulus is higher than the loss modulus which represents the solid-like property. In the crossover region, the storage modulus is lower than the loss modulus which displays the indispensable viscous property for the 3D printing process.

In addition, Fu et al. revealed that GO-based composite inks had a stable viscosity ideal for long-term usage[4], thus promoting the practical application of GO-based 3D printable inks. 3D printing both GO and GO-Si ribbons are shown in Figure 5c, where the ribbon is printed using the pre-programmed design routine and the ink ejects from the nozzle at an appropriate speed due to a controlled air-powered fluid dispenser. The as-printed ribbon can be peeled off the glass substrate in ~5 minutes after printing to obtain a freestanding ribbon. The freestanding GO-based ribbons exhibit exceptional flexibility, as shown in Figure 5c. 3D printed GO ribbon can be bent almost 180° with a tweezers and the GO-Si ribbon can be wound into a spiral shape. After post-treatment procedures such as freeze-drying and thermal reduction of GO to RGO, the binder-free

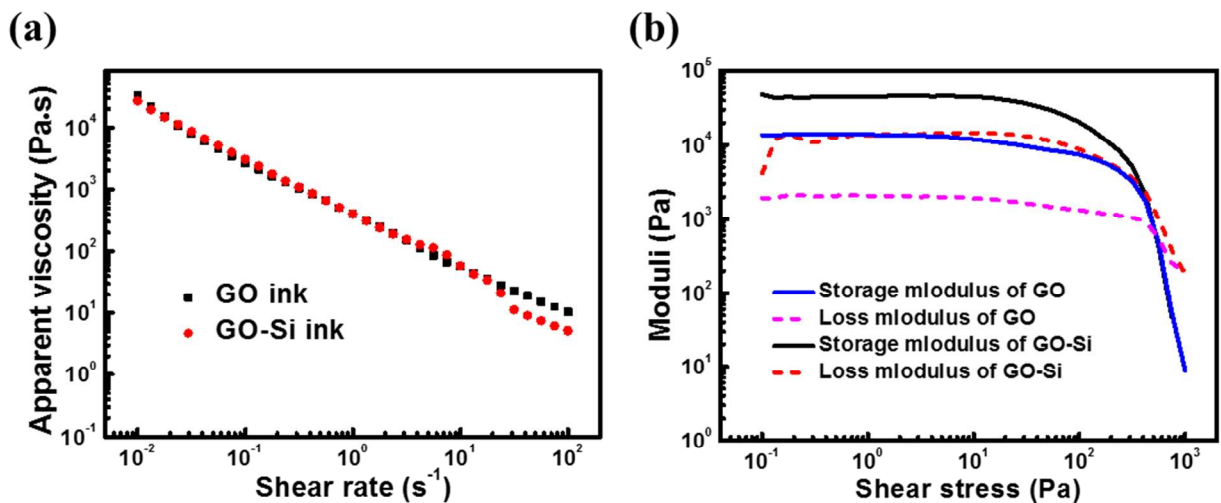RGO or RGO-Si can be directly used to manufacture the RGO-SiNPs nanoarchitectures for use as LIB anodes.

Figure S11. (a) Apparent viscosity as a function of shear rate for GO and GO-Si inks. (b) Storage modulus and loss modulus as a function of shear stress for GO and GO-Si inks.
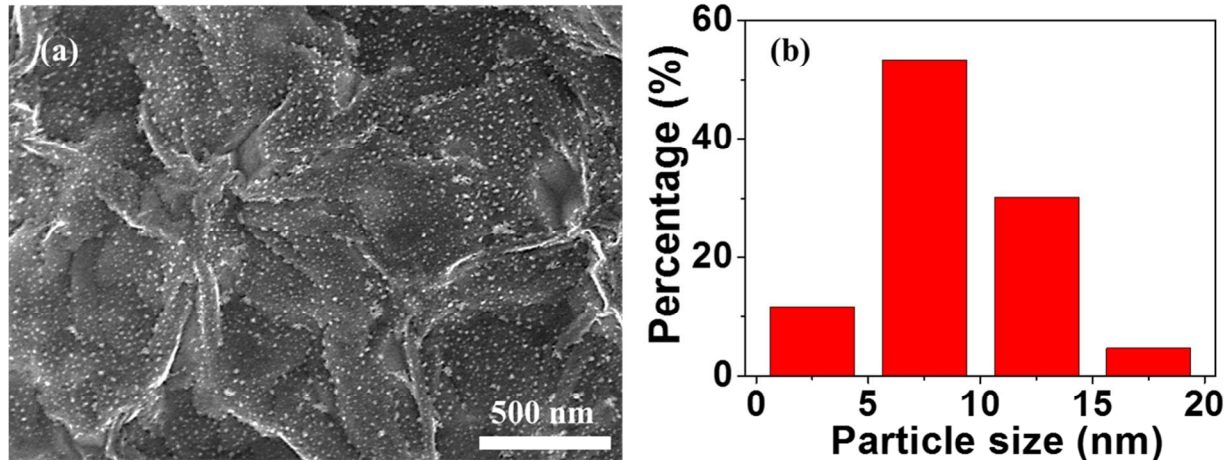

Figure S12. (a) SEM image of RGO-SnNPs. (b) Statistical particle size distribution of SnNPs after thermal shock treatment at ~1550 K for ~1s.

Reference

(1)   Marcano, D. C.; Kosynkin, D. V.; Berlin, J. M.; Sinitskii, A.; Sun, Z.; Slesarev, A.; Alemany, L. B.; Lu, W.; Tour, J. M. *ACS Nano* **2010**, *4* (8), 4806–4814.

(2)   Kim, Y. D.; Kim, H.; Cho, Y.; Ryoo, J. H.; Park, C.-H.; Kim, P.; Kim, Y. S.; Lee, S.; Li, Y.; Park, S.-N.; Shim Yoo, Y.; Yoon, D.; Dorgan, V. E.; Pop, E.; Heinz, T. F.; Hone, J.; Chun, S.-H.; Cheong, H.; Lee, S. W.; Bae, M.-H.; Park, Y. D. *Nat. Nanotechnol.* **2015**, *10* (8), 676–681.

(3)   Freitag, M.; Chiu, H.-Y.; Steiner, M.; Perebeinos, V.; Avouris, P. *Nat. Nanotechnol.* **2010**, *5* (7), 497–501.

(4)   Fu, K.; Wang, Y.; Yan, C.; Yao, Y.; Chen, Y.; Dai, J.; Lacey, S.; Wang, Y.; Wan, J.; Li, T.; Wang, Z.; Xu, Y.; Hu, L. *Adv. Mater.* **2016**.